iScience

CellPress
OPEN ACCESS

Article

The Loss of Nuclear PTEN Increases Tumorigenesis in a Preclinical Mouse Model for Hepatocellular Carcinoma

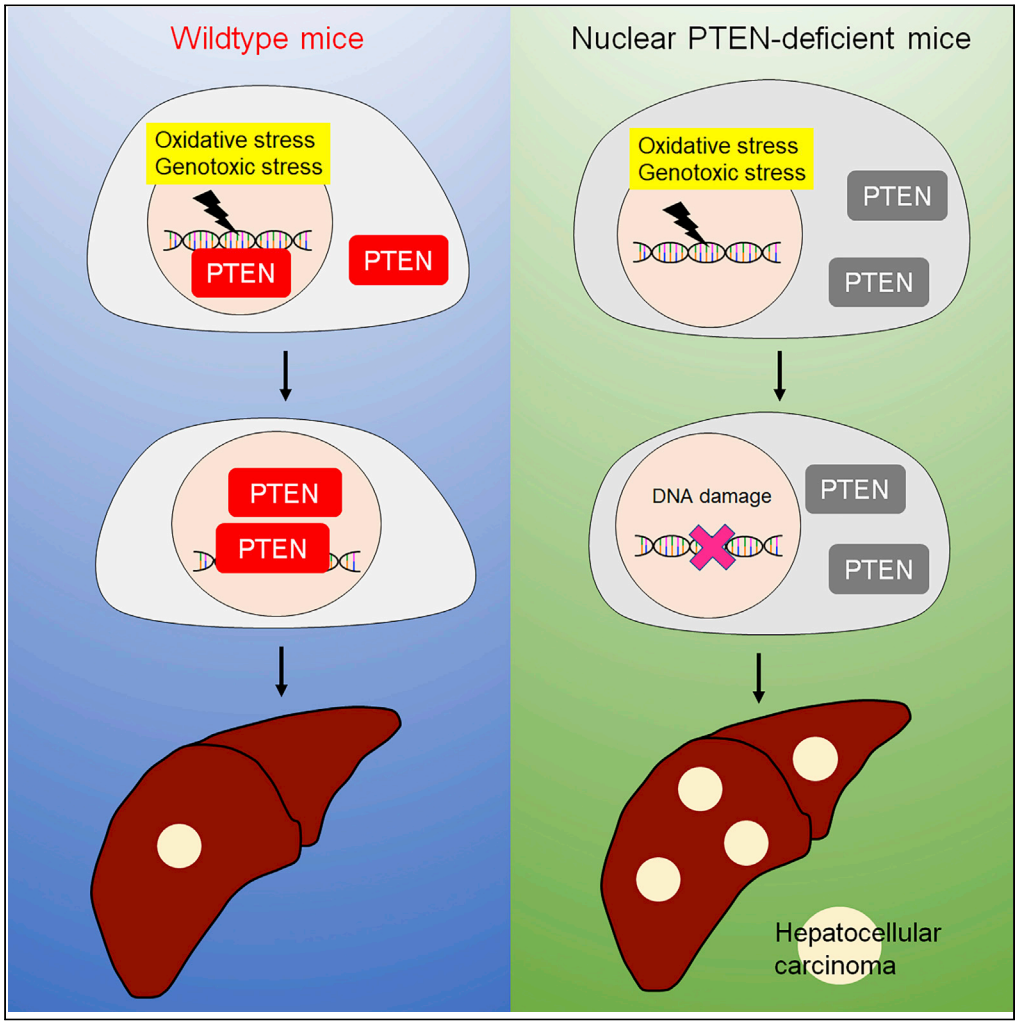

Takashi Kato, Tatsuya Yamada, Hideki Nakamura, Atsushi Igarashi, Robert A. Anders, Hiromi Sesaki, Miho Iijima

miijima@jhmi.edu

HIGHLIGHTS

The nuclear localization of PTEN is regulated by ubiquitination of lysine 13

Nuclear PTEN suppresses DNA damage *in vivo*

Nuclear PTEN loss causes tumorigenesis in a mouse model for hepatocellular carcinoma

Kato et al., iScience *23*, 101548
October 23, 2020
https://doi.org/10.1016/j.isci.2020.101548

iScience

CellPress
OPEN ACCESS

Article

The Loss of Nuclear PTEN Increases Tumorigenesis in a Preclinical Mouse Model for Hepatocellular Carcinoma

Takashi Kato,[1] Tatsuya Yamada,[1] Hideki Nakamura,[1] Atsushi Igarashi,[1] Robert A. Anders,[2] Hiromi Sesaki,[1] and Miho Iijima[1,3,*]

SUMMARY

The *PTEN* gene is highly mutated in many cancers, including hepatocellular carcinoma. The PTEN protein is located at different subcellular regions—PTEN at the plasma membrane suppresses PI3-kinase signaling in cell growth, whereas PTEN in the nucleus maintains genome integrity. Here, using nuclear PTEN-deficient mice, we analyzed the role of PTEN in the nucleus in hepatocellular carcinoma that is induced by carcinogen and oxidative stress-producing hepatotoxin. Upon oxidative stress, PTEN was accumulated in the nucleus of the liver, and this accumulation promoted repair of DNA damage in wild-type mice. In contrast, nuclear PTEN-deficient mice had increased DNA damage and accelerated hepatocellular carcinoma formation. Both basal and oxidative stress-induced localization of PTEN in the nucleus require ubiquitination of lysine 13 in PTEN. Taken together, these data suggest the critical role of nuclear PTEN in the protection from DNA damage and tumorigenesis *in vivo*.

INTRODUCTION

Phosphatase and tensin homolog deleted on chromosome ten (PTEN) is one of the most critical tumor suppressors, which functions at different subcellular locations, including the plasma membrane and nucleus (Baker, 2007; Gil et al., 2007; Hopkins and Parsons, 2014; Kreis et al., 2014; Leslie et al., 2016; Planchon et al., 2008). At the plasma membrane, PTEN counteracts PI3 kinase signaling by dephosphorylating the potent second messenger PIP3 to PIP2. The loss of PTEN in cancer cells results in over-activation of AKT and mTOR signaling, leading to excessive stimulation of cell growth and inhibition of cell death (Chalhoub and Baker, 2009; Endersby and Baker, 2008; Fruman et al., 2017; Iijima and Devreotes, 2002; Iijima et al., 2002; Song et al., 2012). In the nucleus, PTEN functions in DNA repair, genome stability, and cell cycle control through associations with Rad51 and p53 (Baker, 2007; Bassi et al., 2013; Chung et al., 2006; Gil et al., 2007; Kreis et al., 2014; Leslie et al., 2016; Planchon et al., 2008; Shen et al., 2007; Song et al., 2011). PTEN in the nucleus also produces resistance to ionizing radiation therapy (Ma et al., 2019). Most PTEN functions in the nucleus are independent of its lipid phosphatase activity (Baker, 2007; Bassi et al., 2013; Chung et al., 2006; Gil et al., 2007; Kreis et al., 2014; Leslie et al., 2016; Planchon et al., 2008; Shen et al., 2007; Song et al., 2011). Therefore, the loss of PTEN produces multiple effects on the tumorigenesis at different subcellular locations.

The subcellular localization of PTEN is highly regulated (Kreis et al., 2014; Leslie et al., 2016). It has been shown that the recruitment of PTEN to the plasma membrane is regulated by phosphorylation of a cluster of serine and threonine residues at the C-terminal region (Das et al., 2003; Nguyen et al., 2014a, 2014b, 2015a, 2015b; Rahdar et al., 2009; Yang et al., 2017). The phosphorylation controls the conformation of PTEN via intramolecular interactions between the C terminus and the membrane-binding interface. Phosphorylation closes the PTEN conformation by promoting interactions, whereas dephosphorylation opens the PTEN conformation. Also, the C-terminal phosphorylation regulates the localization of PTEN in the nucleus (Nguyen et al., 2014a, 2015b). When the conformation of PTEN is opened, PTEN can accumulate in the nucleus, likely through exposing a nuclear localization signal. It is currently unknown what types of physiological and pathological cues control these conformations of PTEN.

The nuclear localization of PTEN changes in response to various stress. For example, oxidative stress with hydrogen peroxide (H_2O_2) induces the accumulation of PTEN in the nucleus (Chang et al., 2008; Choi et al.,

[1]Department of Cell Biology, Johns Hopkins University School of Medicine, Baltimore, MD, USA

[2]Department of Pathology, Johns Hopkins University School of Medicine, Baltimore, MD, USA

[3]Lead Contact

*Correspondence: miijima@jhmi.edu

https://doi.org/10.1016/j.isci.2020.101548

2013; Hou et al., 2019). Genotoxic stress with ionizing radiation also changes the level of PTEN in the nucleus (Bassi et al., 2013; Ma et al., 2019). The ubiquitination of PTEN has been suggested to be important for the nuclear localization of PTEN at the basal condition; however, it is not well understood whether stress-induced nuclear localization of PTEN is regulated by ubiquitination (Nguyen et al., 2015b; Song et al., 2008; Trotman et al., 2007). In addition to the regulation of the localization of PTEN in the nucleus, the physiological role of nuclear PTEN *in vivo* remains uncertain. Although a study has reported that increased degradation of nuclear PTEN promotes cancer in a xenograft model (Ge et al., 2020), the *in vivo* effect of direct manipulation of PTEN localization on tumorigenesis remains to be determined.

We have recently created a mouse model in which the level of nuclear PTEN is decreased (Igarashi et al., 2018). In the nuclear PTEN-deficient mice, the size of both neurons and brains is decreased, demonstrating the importance of nuclear PTEN in the central nervous system (Igarashi et al., 2018). This brain phenotype is in sharp contrast to increased brain size in mice lacking the total PTEN owing to enhanced PI3-kinase signaling (Backman et al., 2001; Endersby and Baker, 2008; Knobbe et al., 2008; Kwon et al., 2006). Furthermore, unlike the total loss of PTEN, the deficiency of nuclear PTEN did not show spontaneous tumorigenesis (Igarashi et al., 2018). In this report, we analyzed this mouse model to study the role of nuclear PTEN in stress-induced tumorigenesis *in vivo*. We found that nuclear PTEN-deficient mice have increased DNA damage and enhanced formation of hepatocellular carcinoma when the mice are exposed to a carcinogen and hepatotoxin. These data suggest that nuclear PTEN plays an important role in tumorigenesis *in vivo* potentially through preventing DNA damage.

RESULTS

Lysine 13 Is Essential for the Nuclear Accumulation of PTEN

To investigate the mechanism by which PTEN is accumulated in the nucleus in response to oxidative stress, we treated human prostate cancer cell line DU145 and primary mouse hepatocytes with H_2O_2. Immunofluorescence microscopy using anti-PTEN antibodies showed that PTEN is accumulated after the H_2O_2 treatment in both cell types (Figures 1A and 1B). This nuclear accumulation of PTEN was reversible: when ectopically expressed in DU145 cells, PTEN-GFP was first accumulated in the nucleus upon H_2O_2 treatment, similar to endogenous PTEN, and was then re-distributed in the cytosol and nucleus at 6 h after washout of H_2O_2 (Figures 1C and 1D). Similar to H_2O_2, increasing levels of nitric oxide, another reactive oxygen species, with spermine NONOate (SPNO) also induced the nuclear accumulation of PTEN-GFP (Figures 1E and 1F).

Phosphorylation of the C-terminal region of PTEN modulates the conformation of PTEN and regulates its localization to the nucleus and the plasma membrane (Nguyen et al., 2014a, 2015b). Consistent with these previous reports, alanine mutations of the phosphorylation sites (S380, T382, T383, and S385) accumulated $PTEN_{S380A,T382A,T383A,S385A}$ in the nucleus even in the absence of H_2O_2 in human colon cancer cell line HCT116 (Figures 1G and 1H). H_2O_2 did not further increase the nuclear localization of $PTEN_{S380A,T382A,T383A,S385A}$. In contrast, other phospho-defective PTEN mutants, $PTEN_{T319A,T321A}$ and $PTEN_{T366A,S370A}$, behaved similarly to wild-type (WT) PTEN-GFP (Figures 1G and 1H). Western blotting showed that phosphorylation of S380, T382, T383, and S385 was not changed in response to H_2O_2 treatment (Figures 1I and 1J). Therefore, the phosphorylation of the C terminus of PTEN controls its basal nuclear localization and is not regulated by oxidative stress.

It has been suggested that lysine residues are important for the nuclear localization of PTEN (Bassi et al., 2013; Nguyen et al., 2015b; Song et al., 2008; Trotman et al., 2007). Using PTEN-GFP, we asked which lysines are required for PTEN to be accumulated in the nucleus in response to oxidative stress. We first mutated lysines that have been proposed to be subject to post-translational modifications, including K6, K13, K66, K80, K254, K289, and five lysines located in the CBR3 loop (K260, K263, K266, K267, and K269) to arginine (Kreis et al., 2014; Leslie et al., 2016). Substitution of these residues did not change the localization of PTEN in the presence or absence of H_2O_2, except for K13 in HCT116 cells (Figures 2A and 2B). $PTEN_{K13R}$-GFP was excluded from the nucleus before H_2O_2 exposure and failed to accumulate in the nucleus after H_2O_2 exposure. Similar results were obtained when we tested PTEN-GFP and $PTEN_{K13R}$-GFP in human hepatocarcinoma cell line HepG2 (Figures 2C and 2D). These data suggest that K13 is a key lysine that controls the nuclear localization of PTEN. Although PTEN has been shown to dimerize (Papa et al., 2014), we found no effects of endogenous PTEN (regardless of presence or absence of PTEN) on the distribution of WT PTEN-GFP or $PTEN_{K13R}$-GFP in response to H_2O_2 in three cell lines,

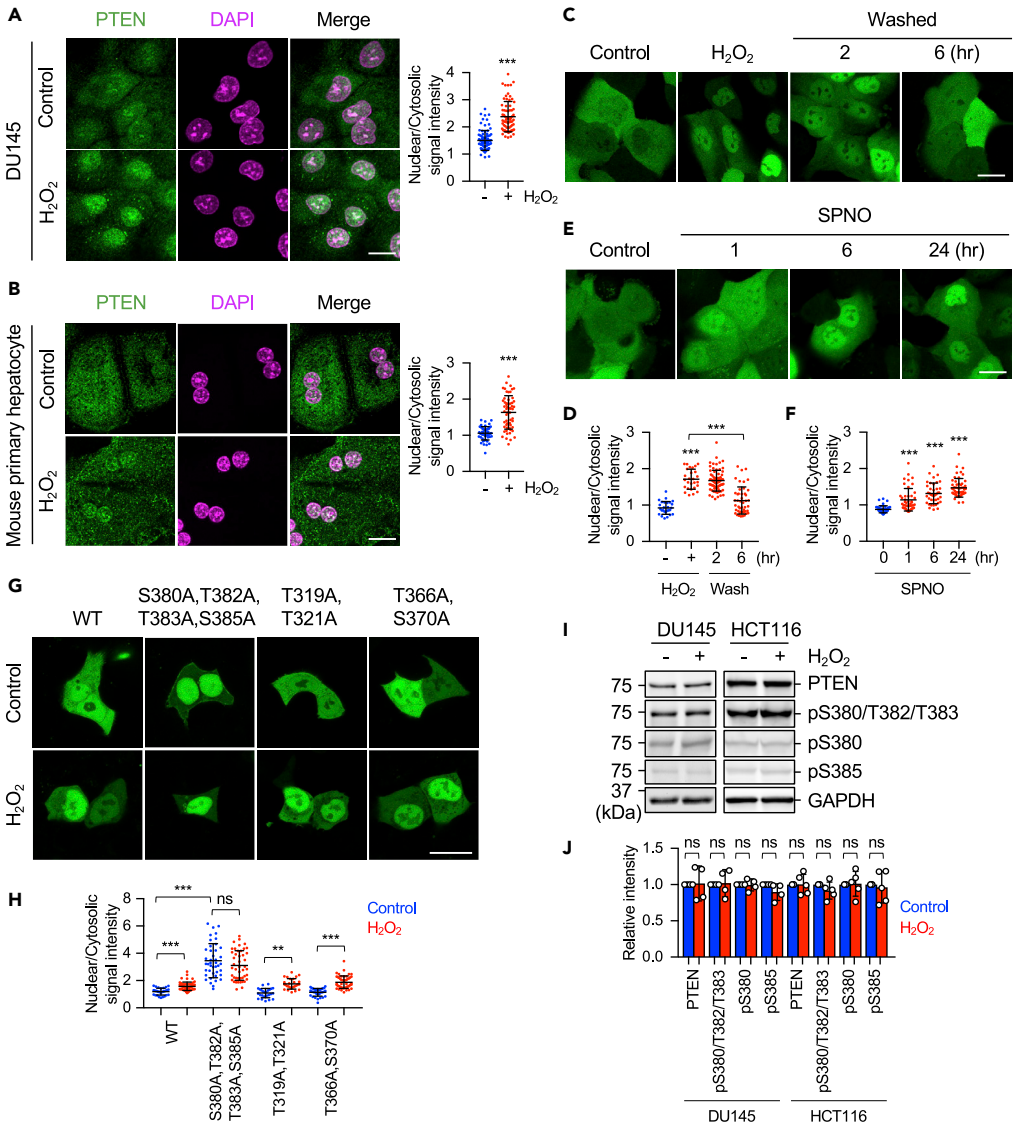

Figure 1. Oxidative Stress Induces the Accumulation of PTEN in the Nucleus

(A and B) DU145 cells (A) and mouse primary hepatocytes (B) were treated with 0.5 mM H_2O_2 for 1 h. Immunofluorescence microscopy using anti-PTEN antibodies was performed. Nuclear DNA was stained with DAPI. The intensity of the PTEN signal in the nucleus was quantified relative to that in the cytosol. Bars are average ± SD (n = 52–84 cells).

(C and D) DU145 cells expressing GFP-PTEN were treated with 0.5 mM H_2O_2 for 1 h. After washes, cells were incubated in the culture medium without H_2O_2 for 6 h. Live cell imaging was performed using confocal microscopy. The intensity of GFP in the nucleus was quantified relative to that in the cytosol in (D). Bars are average ± SD (n = 27–74 cells).

(E and F) DU145 cells expressing PTEN-GFP were treated with 400 μM SPNO for the indicated amounts of time and observed by confocal microscopy. The intensity of GFP in the nucleus was quantified relative to that in the cytosol in (F). Bars are average ± SD (n = 40–52 cells).

(G and H) HCT116 cells expressing GFP fused to phosphorylation defective PTEN mutants were treated with 0.5 mM H_2O_2 for 1 h. The intensity of GFP in the nucleus was quantified relative to that in the cytosol in (H). Bars are average ± SD (n = 25–55 cells).

(I and J) DU145 and HCT116 cells were treated with 0.5 mM H_2O_2 for 1 h and analyzed by western blotting. The PTEN and phosphorylated PTEN band intensities were quantified relative to those of GAPDH and PTEN, respectively, in (J). Bars are average ± SD (n = 4–5). Statistical analysis was performed using Student's t test in (A, B, and J) and one-way ANOVA with post hoc Tukey in (D, F, and H): $^{**}p < 0.01$, $^{***}p < 0.001$. Scale bars, 20 μm.

See also Table S1.

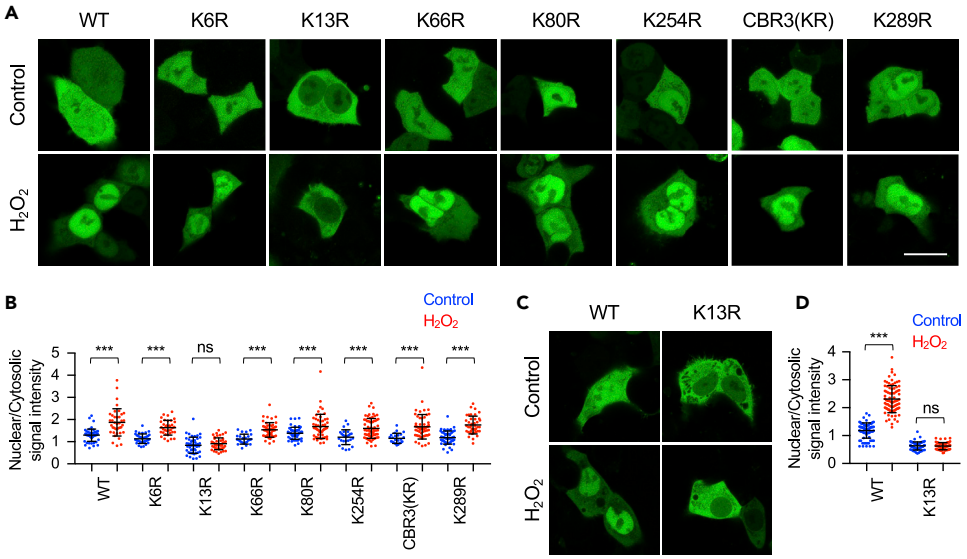

Figure 2. Lysine 13 is Critical for the Nuclear Localization of PTEN

(A and B) HCT116 cells expressing GFP fused to PTEN lysine mutants were treated with 0.5 mM H_2O_2 for 1 h. The intensity of GFP in the nucleus was quantified relative to that in the cytosol in (B). Bars are average ± SD (n = 23–63 cells).

(C and D) HepG2 cells expressing PTEN-GFP or $PTEN_{K13R}$-GFP were treated with 0.5 mM H_2O_2 for 1 h. The intensity of GFP in the nucleus was quantified relative to that in the cytosol in (D). Bars are average ± SD (n = 58–83 cells). Statistical analysis was performed using one-way ANOVA with post hoc Tukey in (B and D): ***$p < 0.001$.

See also Figure S1 and Table S1.

which carry two copies (HCT116 cells), one copy (DU145 cells), or no copy (human prostate cancer cell line PC3) of PTEN (Figure S1).

To further test whether all other lysines regulate PTEN's nuclear localization, we replaced all 34 lysines to arginines in PTEN, creating $PTEN_{K0}$ (Figures 3A and 3B). $PTEN_{K0}$-GFP was greatly excluded from the nucleus in the presence or absence of H_2O_2, similar to $PTEN_{K13R}$-GFP (Figures 3C and 3D). We then put back K13 in $PTEN_{K0}$ and created $PTEN_{K0K13}$. $PTEN_{K0K13}$-GFP restored both basal nuclear localization and H_2O_2-induced nuclear accumulation (Figures 3C and 3D). These data show that K13 is the major lysine residue that controls the nuclear localization of PTEN in response to oxidative stress.

To ask if K13 undergoes ubiquitination, we expressed HA-ubiquitin along with WT PTEN-GFP, $PTEN_{K0}$-GFP, or $PTEN_{K0K13}$-GFP in HEK293T cells and immunoprecipitated using GFP-Trap beads. Western blotting showed that WT PTEN-GFP is at least mono-, bi-, and tri-ubiquitinated under the basal condition, and these ubiquitinations are dramatically decreased in $PTEN_{K0}$-GFP (Figures 4A and 4B). The majority of ubiquitination was restored in $PTEN_{K0K13}$-GFP (Figures 4A and 4B). Also, we found that mono-, bi-, and tri-ubiquitinations of WT PTEN-GFP are increased in response to H_2O_2 treatment (Figures 4C and 4D). In contrast, $PTEN_{K13R}$-GFP showed decreases in H_2O_2 induced bi- and tri-ubiquitinations (Figures 4C and 4D). These data suggest that K13 is the major site of ubiquitination in PTEN under both basal and oxidative stress conditions.

To determine whether artificial fusion of ubiquitin to PTEN can replace the role of K13 for the nuclear localization, we placed ubiquitin between residue 12 and 14 (lysine 13 was removed) in PTEN-GFP and expressed $PTEN_{K13}$-Ubi-GFP in HEK293T cells (Figure 4E). $PTEN_{K13}$-Ubi-GFP restored both the basal nuclear localization and the nuclear accumulation in response to H_2O_2, similar to WT PTEN-GFP (Figures 4F and 4G). Therefore, the ubiquitination of K13 is important for the nuclear localization of PTEN.

If the ubiquitination of PTEN is critical for its nuclear localization, inhibiting de-ubiquitination might promote this localization. Indeed, when treated with a broad inhibitor to de-ubiquitination enzymes, PR-619, PTEN-GFP was accumulated in the nucleus without H_2O_2 (Figures 4H and 4I). This PR-619-induced nuclear accumulation depends on K13 since both $PTEN_{K13R}$-GFP and $PTEN_{K0}$-GFP did not accumulate in the nucleus in the presence of PR-619 (Figures 4H and 4I). Furthermore, $PTEN_{K0K13}$-GFP restored the PR-619-

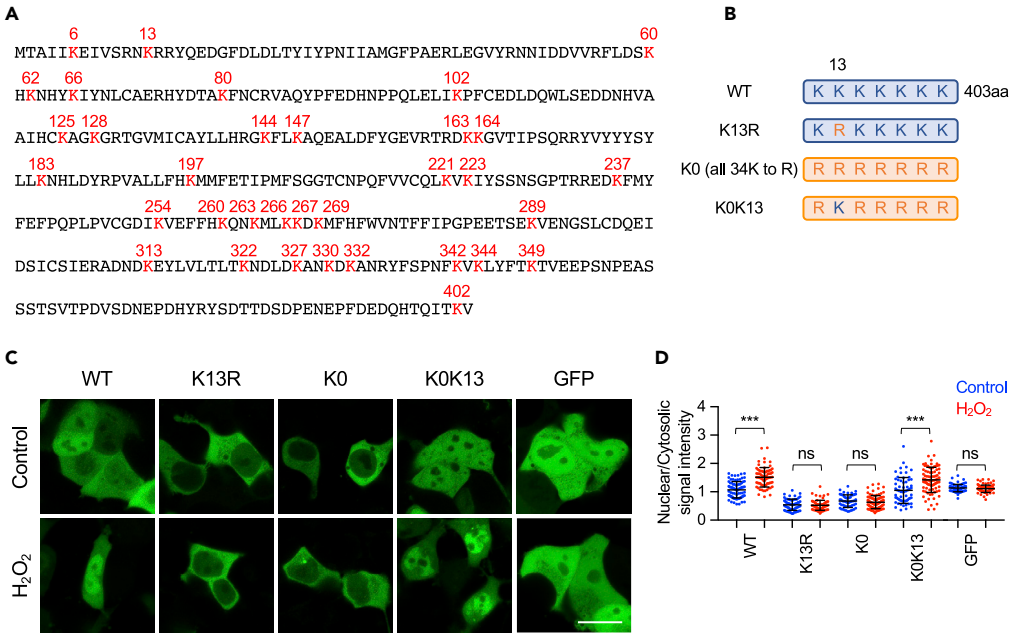

Figure 3. Lysine 13 is Sufficient for the Nuclear Localization of PTEN

(A) Lysine residues in PTEN. PTEN contains 34 lysines.

(B) Schematic diagrams of PTEN constructs. In the K0 mutant, all 34 lysines were changed to arginine. In the K0K13 mutant, all 34 lysines were changed to arginine expect for lysine 13.

(C and D) HEK293T cells expressing the indicated PTEN-GFP mutants were treated with 0.5 mM H_2O_2 for 1 h. The intensity of GFP in the nucleus was quantified relative to that in the cytosol in (D). Bars are average ± SD (n = 57–88 cells). Student's t test: ***p < 0.001. Scale bars, 20 μm.

See also Table S1.

induced nuclear accumulation (Figures 4H and 4I). These data further support the importance of the ubiquitination of K13 in the nuclear localization of PTEN.

Reactive oxygen species create DNA damage in the nucleus. To test whether DNA damage induces nuclear accumulation of PTEN, we treated cells with a topoisomerase inhibitor, camptothecin. We found that camptothecin induces the nuclear accumulation of WT PTEN-GFP in HEK293T (Figures 5A and 5B), HepG2 (Figures 5C and 5D), HCT116 (Figure S1), DU145 (Figure S1), and PC3 (Figure S1) cells. In contrast, $PTEN_{K13R}$-GFP was unable to accumulate in the nucleus in the presence of camptothecin in all of these five cells (Figures 5A–5D and S1). Therefore, K13 is important for the nuclear accumulation of PTEN induced by DNA damage.

To test whether antioxidants can block the nuclear accumulation of PTEN in response to reactive oxygen species and DNA damage, we treated HCT116 cells expressing PTEN-GFP with either H_2O_2 or camptothecin in the presence of glutathione monoethyl ester (GSH-MEE). GSH-MEE significantly blocked the nuclear accumulation of PTEN induced by H_2O_2 (Figures 6A and 6B). In contrast, GSH-MEE was not able to block the nuclear recruitment of PTEN induced by camptothecin (Figures 6C and 6D). These data suggest that reactive oxygen species cause DNA damage and then promote nuclear PTEN localization.

Dynamics of Nuclear Import and Export of PTEN

Live cell imaging of PTEN-GFP showed that WT PTEN-GFP gradually accumulated in the nucleus after H_2O_2 treatment (Figures 7A and 7B). In contrast, $PTEN_{K13R}$-GFP remained in the cytosol after H_2O_2 treatment (Figures 7A and 7B). To determine how the K13R mutation affects the dynamics of PTEN's localization, we tagged a marker protein, mEos (Zhang et al., 2012), to PTEN and expressed PTEN-mEos in DU145 cells. mEos is a monomeric form of an Eos fluorescent protein with UV-inducible green to red color conversion (Zhang et al., 2012) When we photoconverted PTEN-mEos in the cytosol, a fraction of photoconverted PTEN-mEos was imported into the nucleus (Figures 7C, 7E, and 7G). Treatment with H_2O_2 did not affect the rate of the nuclear import of PTEN-mEos (Figures 7C, 7E, and 7G). In contrast, when we measured the rate of nuclear export by

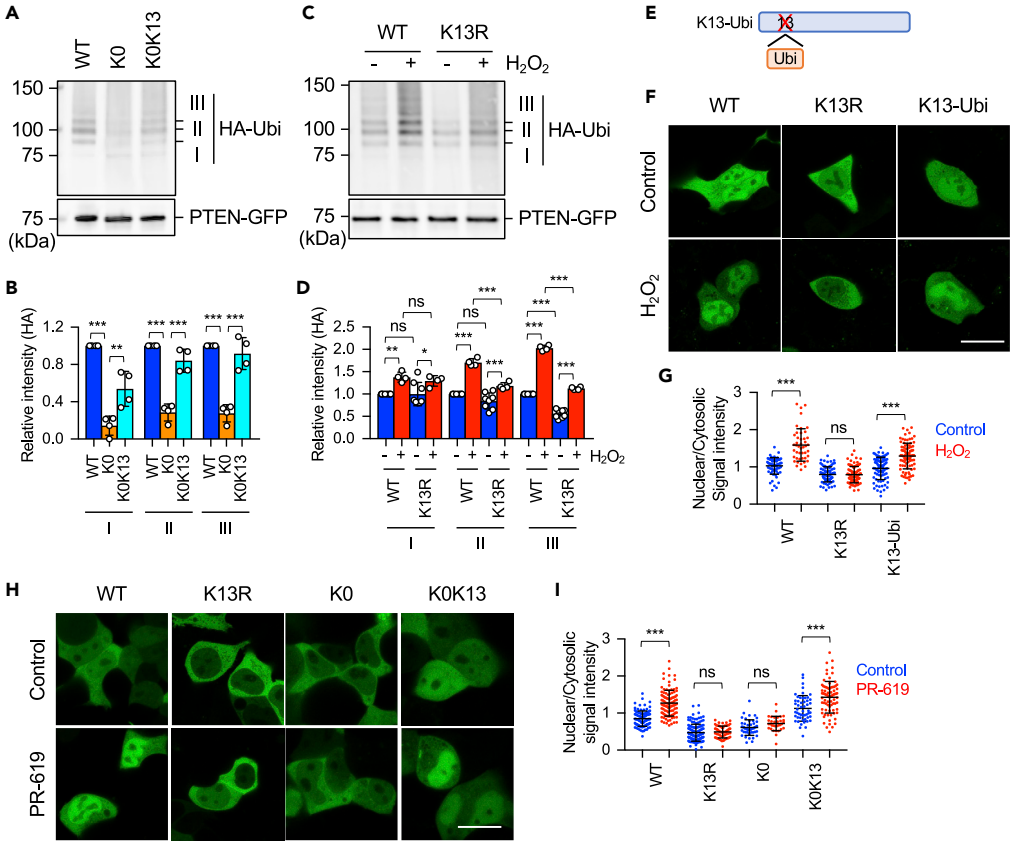

Figure 4. The Ubiquitination of Lysine 13 Controls the Nuclear Localization of PTEN in Response to H_2O_2

(A and B) Whole-cell lysates of HEK293T cells expressing HA-ubiquitin along with the indicated PTEN-GFP constructs were incubated with GFP-Trap. The pellet fractions were analyzed by western blotting using antibodies to GFP and HA. Mono-, bi-, and tri-ubiquitination of PTEN-, $PTEN_{K0}$-, and $PTEN_{K0K13}$-GFP were quantified relative to that of PTEN-, $PTEN_{K0}$-, and $PTEN_{K0K13}$-GFP in (B). Bars are average ± SD (n = 4).

(C and D) HEK293T cells carrying HA-ubiquitin along with GFP-PTEN or $PTEN_{K13R}$-GFP were treated with 0.5 mM H_2O_2 for 1 h. PTEN-GFP and $PTEN_{K13R}$-GFP were pulled down using GFP-Trap beads. The pellet fractions were analyzed by western blotting using antibodies to GFP and HA. Ubiquitination was quantified in (D). Bars are average ± SD (n = 4–8).

(E) K13 was replaced by ubiquitin in $PTEN_{K13\text{-}Ubi}$.

(F and G) HCT116 cells expressing PTEN-GFP, $PTEN_{K13R}$-GFP, or $PTEN_{K13\text{-}Ubi}$-GFP were treated with 0.5 mM H_2O_2 for 1 h. Live cell imaging was performed using confocal microscopy. The intensity of GFP in the nucleus was quantified relative to that in the cytosol in (G). Bars are average ± SD (n = 45–91 cells).

(H and I) HEK293T cells carrying the indicated PTEN constructs were treated with 15 μM PR-619, a broad-range reversible and cell-permeable inhibitor of the deubiquitylating enzyme, for 2 h. The intensity of GFP in the nucleus was quantified relative to that in the cytosol (I). Bars are average ± SD (n = 33–134 cells). Statistical analysis was performed using one-way ANOVA with post hoc Tukey in (B, D, G, and I): $^{**}p < 0.01$, $^{***}p < 0.001$. Scale bars, 20 μm.

See also Table S1.

photoconverting PTEN-mEos in the nucleus, nuclear export was significantly decreased by H_2O_2 (Figures 7D, 7F, and 7G). These data suggest that the H_2O_2-induced nuclear accumulation of PTEN is achieved by decreasing the nuclear export rate without changing the nuclear import rate (Figure 7H).

The rate of the nuclear import of $PTEN_{K13R}$-mEos was much lower than that of WT PTEN-mEos in the absence of H_2O_2 (Figures 7C, 7E, and 7G). This lower rate of import of $PTEN_{K13R}$-mEos was unchanged upon H_2O_2 (Figures 7C, 7E, and 7G). The rate of nuclear export of $PTEN_{K13R}$-mEos was also lower than that of WT PTEN-mEos and did not change in response to H_2O_2 (Figures 7D, 7F, and 7G). Therefore, defects in the nuclear accumulation of $PTEN_{K13R}$ in the nucleus likely result from decreased rates of nuclear import, and oxidative stress does not change the export rate of $PTEN_{K13R}$. Therefore, the majority of $PTEN_{K13R}$ remains in the cytosol regardless of oxidative stress (Figure 7H).

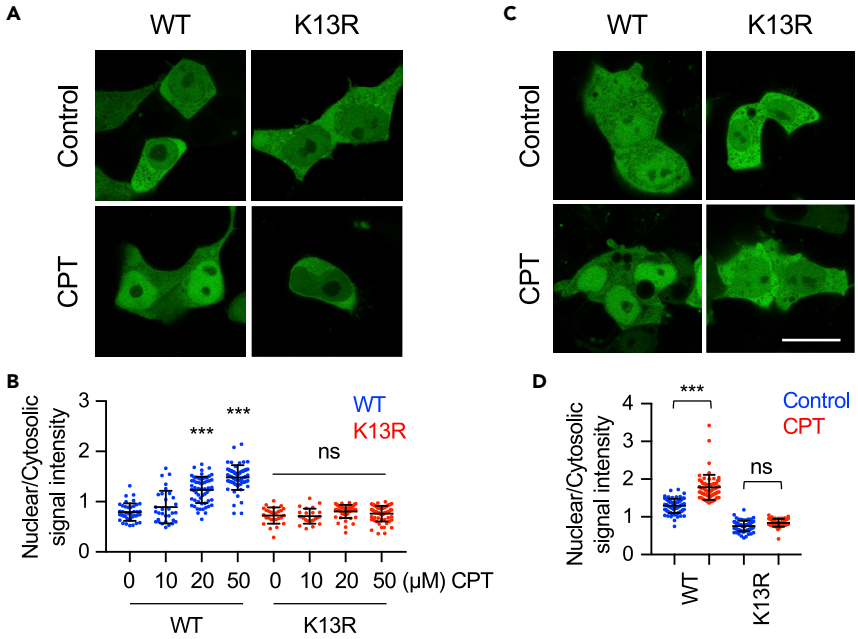

Figure 5. Lysine 13 is Necessary for the Nuclear Localization of PTEN in Response to Camptothecin

(A and B) HEK293T cells expressing the indicated PTEN-GFP constructs were treated with 0, 10, 20, and 50 μM camptothecin (a topoisomerase inhibitor) for 6 h. An image of cells treated with 50 μM camptothecin is presented. The intensity of GFP in the nucleus was quantified relative to that in the cytosol in (B). Bars are average ± SD (n = 24–63 cells). (C and D) HepG2 cells expressing PTEN-GFP or $PTEN_{K13R}$-GFP were treated with 0 (DMSO) or 50 μM camptothecin for 6 h. The intensity of GFP in the nucleus was quantified relative to that in the cytosol in (D). Bars are average ± SD (n = 61–79 cells). Statistical analysis was performed using one-way ANOVA with post hoc Tukey in (B and D): ***p < 0.001. Scale bars, 20 μm.

See also Table S1.

Oxidative Stress-Induced Nuclear Localization of PTEN Is Decreased in the Liver of Nuclear PTEN-Deficient Mice

To examine the nuclear localization of PTEN *in vivo*, we used a hepatotoxin, carbon tetrachloride (CCl_4), which produces oxidative stress in the liver (Recknagel et al., 1989; Sheweita et al., 2001). CCl_4 was intraperitoneally injected into WT mice and nuclear PTEN-deficient mice, in which the *Pten* gene had been edited to carry the K13R and D384V mutations using the CRISPR-Cas9 system (Figure 8A) (Igarashi et al., 2018). We have previously shown that the combination of K13R and mutations that block phosphorylation of the C-terminal tail, such as D384V, more effectively inhibits the localization of PTEN in the nucleus compared with the single K13R mutation (Igarashi et al., 2018; Nguyen et al., 2015b). Indeed, the K13R and D384V mutations specifically decreased the level of PTEN in the nucleus without affecting the level of PTEN in the cytosol (Figures 8B and 8C). Livers were subjected to immunofluorescence microscopy with anti-PTEN antibodies at 0, 2, 4, and 7 days after the CCl_4 injection. In WT mice, without CCl_4 injection, PTEN is located both in the cytosol and nucleus (Figures 8D and 8E). Upon CCl_4 injection, PTEN was accumulated in the nucleus with a peak at day 2 and gradually returned to the normal distribution at day 7 (Figure 8E). In contrast, PTEN in nuclear PTEN-deficient mice showed a decreased level of nuclear localization before CCl_4 injection and remained unchanged in the nucleus after the CCl_4 injection (Figures 8D and 8E). Therefore, PTEN is accumulated in the nucleus *in vivo* in response to oxidative stress, similar to cultured cells *in vitro*, and nuclear accumulation is blocked in nuclear PTEN-deficient mice.

DNA Damage Is Increased in Nuclear PTEN-Deficient Livers in Response to Oxidative Stress

To examine the effect of nuclear PTEN deficiency on DNA damage in the liver, liver sections were analyzed by immunofluorescence microscopy with antibodies to phosphorylated histone 2AX (phospho-H2AX), which is a well-established marker for DNA damage (Bassi et al., 2013), after injection of CCl_4. We measured the signal intensity of phospho-H2AX in each nucleus in the liver. Without CCl_4 injection, we barely detected phospho-H2AX in both WT and nuclear PTEN-deficient mice (Figures 8F and 8G). After CCl_4 injection, the signal intensity of phospho-H2AX in the nucleus was increased with a peak at day 2 and then

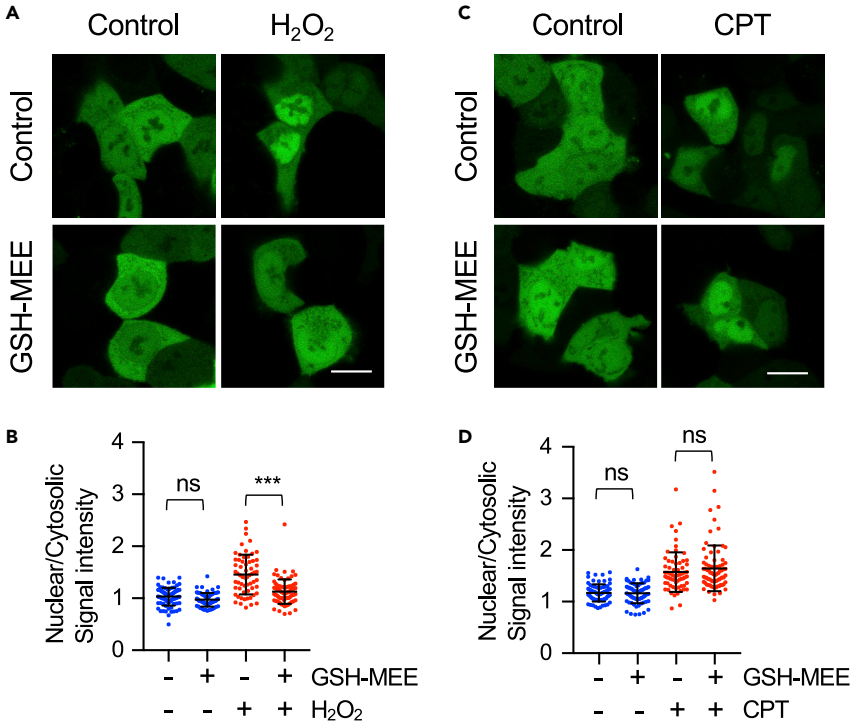

Figure 6. The Effect of an Antioxidant on the Nuclear Localization of PTEN

(A–D). After preincubation with 5 mM GSH-MEE for 16 h, HCT116 cells expressing PTEN-GFP were treated with 0.5 mM H_2O_2 for 1 h (A and B) or 50 μM camptothecin for 6 h (C and D). The intensity of GFP in the nucleus was quantified relative to that in the cytosol in (B and D). Bars are average ± SD (n = 61–84 cells). Statistical analysis was performed using one-way ANOVA with post hoc Tukey in (B and D): ***p < 0.001. Scale bars, 20 μm.

See also Table S1.

decreased at day 4 in WT mice (Figures 8F and 8G). At day 2, nuclear PTEN-deficient mice showed a significantly higher signal intensity of phospho-H2AX, compared with WT mice (Figures 8F and 8G). Supporting these immunofluorescence data, western blotting of livers also revealed an increased level of phospho-H2AX in nuclear PTEN-deficient mice at day 2 (Figures 8H and 8I). As control experiments, we measured serum levels of alanine aminotransferase as a readout for liver damage and found similar activities in WT and nuclear PTEN-deficient mice before and after CCl_4 injection (Figure 8J). Therefore, equivalent damages were produced in the liver of these mice by CCl_4 injection. These data suggest that nuclear PTEN decreases DNA damage in response to oxidative stress *in vivo*.

When we analyzed oncogenic signaling pathways by western blotting of livers, we found similar levels of phosphorylation of ERK, AKT, S6, and GSK-3α/β in WT and PTEN-deficient mice (Figure 9). We also found normal insulin-stimulated AKT phosphorylation in the liver and glucose uptake in nuclear PTEN-deficient mice (Figure 10). Thus, nuclear PTEN-deficient mice show normal signaling involving AKT and ERK in the liver.

Increased Hepatocellular Carcinoma in Nuclear PTEN-Deficient Mice in Response to Oxidative Stress

To test whether nuclear PTEN suppresses tumorigenesis *in vivo*, we used a preclinical mouse model of hepatocellular carcinoma induced by a single injection of a carcinogen, N-nitrosodiethylamine (DEN), followed by repeated injection of the hepatotoxin CCl_4 (Heindryckx et al., 2009; Uehara et al., 2014). We intraperitoneally injected DEN at 2 weeks of age and subsequently injected CCl_4 twice per week from 6 to 14 weeks of age (Figure 11A). We found similar body and liver weights in WT and nuclear PTEN-deficient mice with or without DEN and CCl_4 treatments (Figures 11B and 11C).

In male WT mice, the DEN and CCl_4 treatments induced hepatocellular carcinoma at 15 weeks (Figures 11D–11G), as previously reported (Heindryckx et al., 2009; Uehara et al., 2014). We found increases in

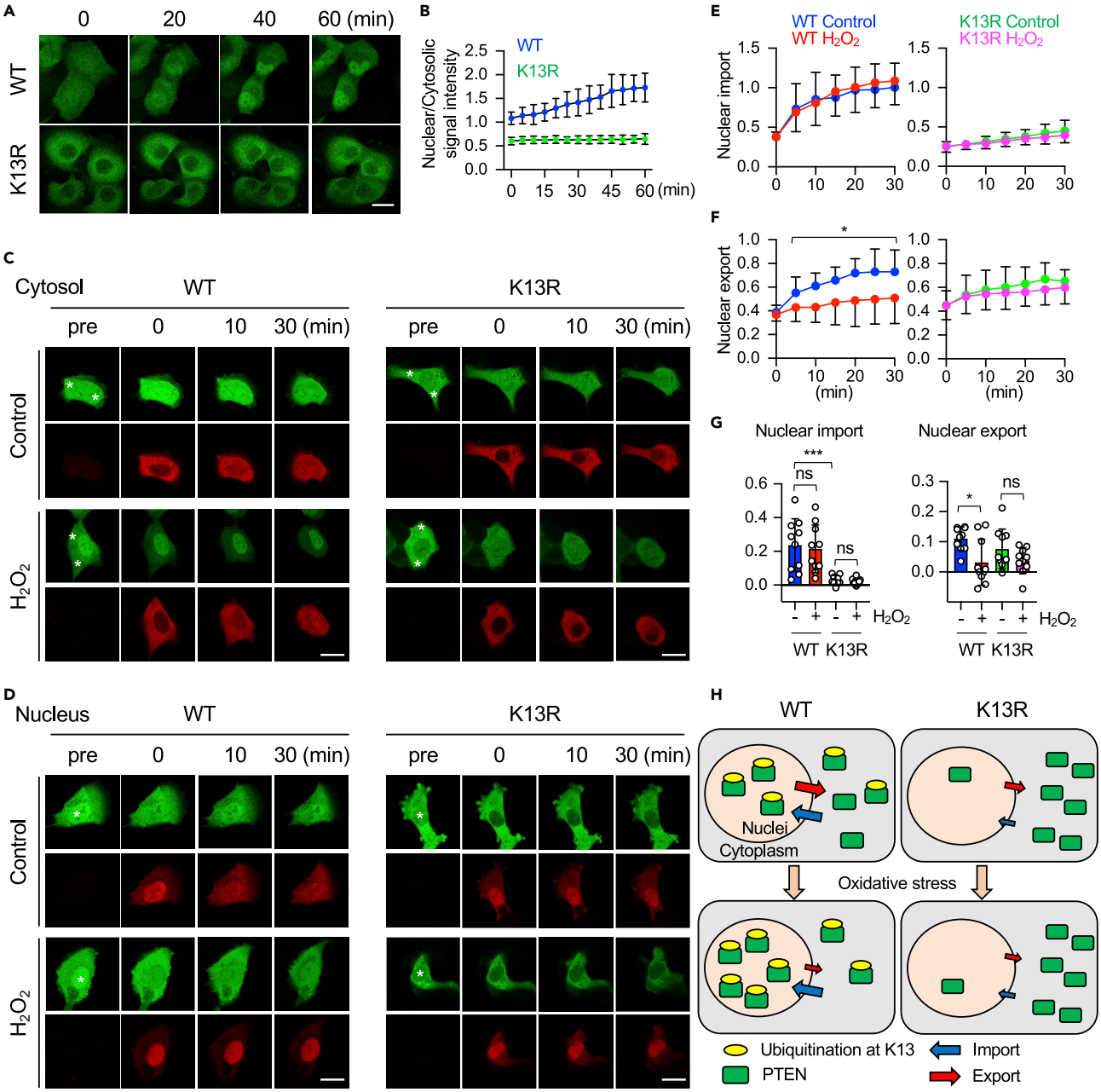

Figure 7. Time-Lapse Analysis of PTEN Localization

(A and B) DU145 cells expressing PTEN-GFP or $PTEN_{K13R}$-GFP were treated with 0.5 mM H_2O_2 for 1 h and analyzed by time-lapse confocal microscopy. The intensity of GFP in the nucleus was quantified relative to that in the cytosol in (B). Bars are average ± SD (n = 20 cells for PTEN-GFP and 22 cells for $PTEN_{K13R}$-GFP).

(C–G) DU145 cells were transfected with plasmids carrying PTEN- or $PTEN_{K13R}$-mEOS. mEos in the two regions of the cytosol in (C) or in the region of the nucleus in (D) was photoconverted using a 405-nm laser on laser scanning confocal microscope (indicated by asterisks). Images were obtained for both photoconverted and unconverted mEos signals in the presence or absence of 0.5 mM H_2O_2 for 30 min. Images before the photoconversion were also obtained (pre). The intensity of photoconverted mEos in the nucleus relative to that in the cytosol (in C and E, to measure the nuclear import of PTEN) and in the cytosol relative to that in the nucleus (in D and F, to measure the nuclear export of PTEN) was quantified. Bars are average ± SD (n = 10–12 cells). Rates of nuclear import and export are calculated in (G).

(H) Summary of the data. Statistical analysis was performed using one-way ANOVA with post hoc Tukey in (G): *p < 0.05, ***p < 0.001. Scale bars, 20 μm. See also Table S1.

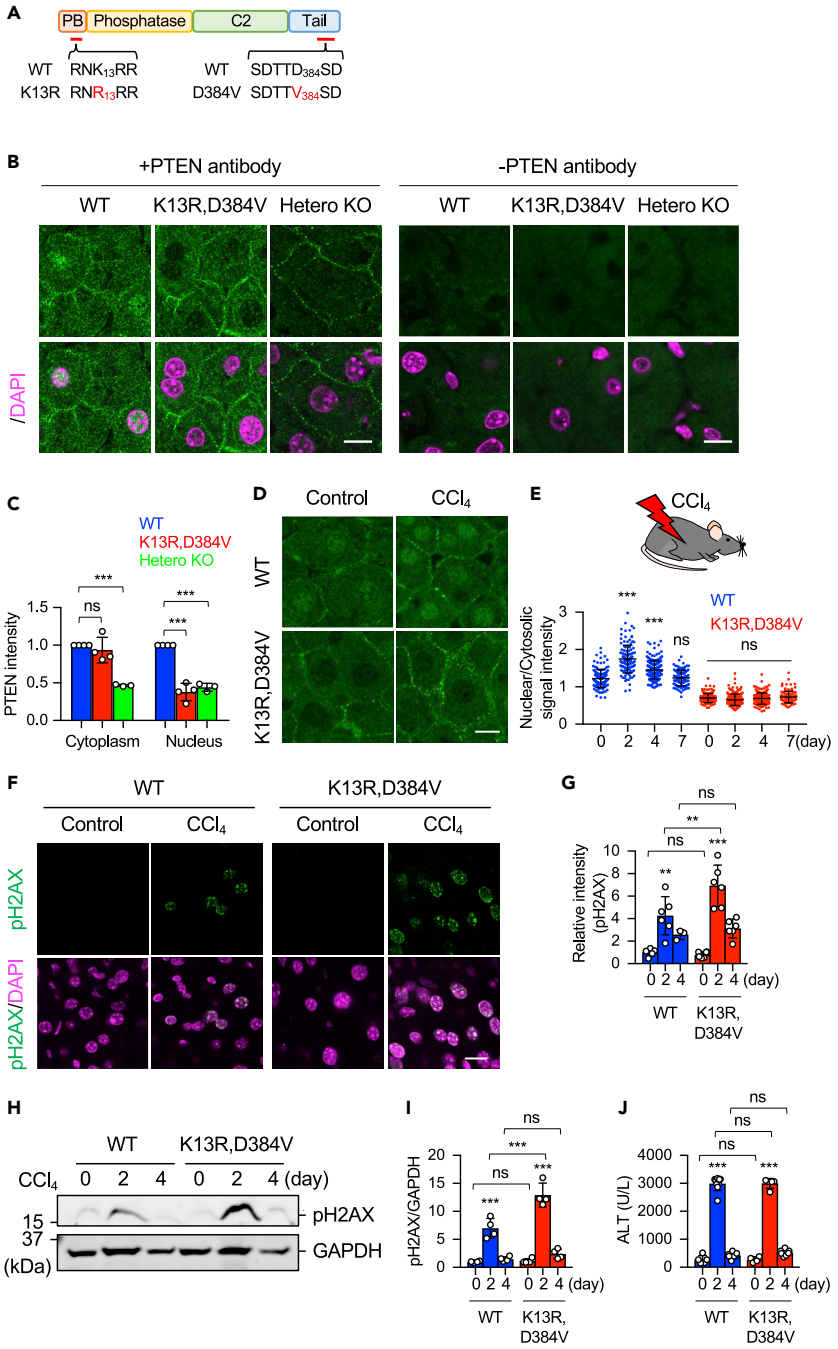

Figure 8. Oxidative Stress Induces the Nuclear Accumulation of PTEN in the Liver

(A) Nuclear PTEN-deficient mice carry K13R and D384V mutations. WT and nuclear PTEN-deficient mice were subjected to intraperitoneal injection of 20% CCl_4/mineral oil (10 mL/kg body weight) at 2–3 months of age.

(B) Liver sections from WT, nuclear PTEN-deficient mice, and heterozygous PTEN knockout mice were placed on the same slides and subjected to immunofluorescence microscopy with (left panel) or without (right panel) the primary antibody.

(C) The intensity of PTEN signals in the cytosol and nucleus was determined after the subtraction of the nonspecific background signal based on the intensity in samples without the primary antibody. Bars are average ± SD (n = 3–4 mice).

(D and E) (D) At 2 days after CCl_4 injection, frozen liver sections were analyzed by immunofluorescence microscopy using anti-PTEN antibodies. The intensity of PTEN signals in the nucleus was quantified relative to that in the cytosol at the indicated days after CCl_4 injection in (E). Bars are average ± SD (n = 101–202 cells).

Figure 8. *Continued*

(F and G) (F) At 2 days after CCl_4 injection, frozen liver sections were analyzed by immunofluorescence microscopy using anti-phospho-H2AX (serine139) antibodies along with DAPI staining. The intensity of phospho-H2AX signals in the nucleus was quantified at the indicated days after CCl_4 injection in (G). Bars are average ± SD (n = 3–6 livers).
(H and I) Livers were isolated from WT and nuclear PTEN-deficient mice at the indicated days after CCl_4 injection and analyzed by western blotting with antibodies to phospho-H2AX and GAPDH. The intensity of phospho-H2AX signals was quantified relative to that of GAPDH in (I). Bars are average ± SD (n = 4 livers).
(J) Serum ALT levels were measured at the indicated days after CCl_4 injection (n = 4–9 mice). Statistical analysis was performed using one-way ANOVA with post hoc Tukey in (C), (E), (G), (I), and (J): $^{**}p < 0.01$, $^{***}p < 0.001$. Scale bars, 20 μm.

both the number of hepatocellular carcinomas and the size of the largest tumors in nuclear PTEN-deficient mice (Figures 11E and 11F). It has been shown that female mice are protected from DEN-induced hepatocarcinogenesis owing to estrogen-mediated inhibition of interleukin-6 (Naugler et al., 2007). Indeed, we found a much higher level of hepatocellular carcinoma in male WT mice compared with female WT mice, in which hepatocellular carcinoma was almost undetectable (Figure 11E). Female nuclear PTEN-deficient mice modestly increased hepatocellular carcinoma compared with female WT mice, but this difference did not reach statistical significance (Figures 11E and 11F). Without the treatment with DEN and CCl_4, no hepatocellular carcinoma was observed in WT and nuclear PTEN-deficient mice regardless of their sex (Figures 11D and 11E).

DEN and CCl_4 treatments induce fibrosis, as in human patients with hepatocellular carcinoma (Heindryckx et al., 2009; Uehara et al., 2014). We found similar levels of fibrosis in male WT and nuclear PTEN-deficient mice using Sirius red stain of liver sections (Figures 11H and 11I). Therefore, liver injuries produced by DEN and CCl_4 treatments were similar in WT and nuclear PTEN-deficient mice. In addition, Ki67 immunostaining showed similar percentages of Ki67-positive cells in regions of hepatocellular carcinoma in male WT and nuclear PTEN-deficient mice (Figures 11J and 11K). Furthermore, immunostaining with antibodies to active caspase-3 revealed similar levels of apoptosis in response to CCl_4 in WT and nuclear PTEN-deficient mice (Figures 11L and 11M). No detectable apoptosis was observed in normal regions and tumors in WT and nuclear PTEN-deficient mice at the basal level (Figures 11L and 11M). These data suggest that hepatocellular carcinoma grows at similar rates without gross apoptosis in WT and nuclear PTEN-deficient mice once they are formed and that the loss of nuclear PTEN increases the frequency of the onset of tumorigenesis. Thus, nuclear PTEN functions as a tumor suppresser and protects against oxidative stress-induced hepatocellular carcinoma *in vivo*.

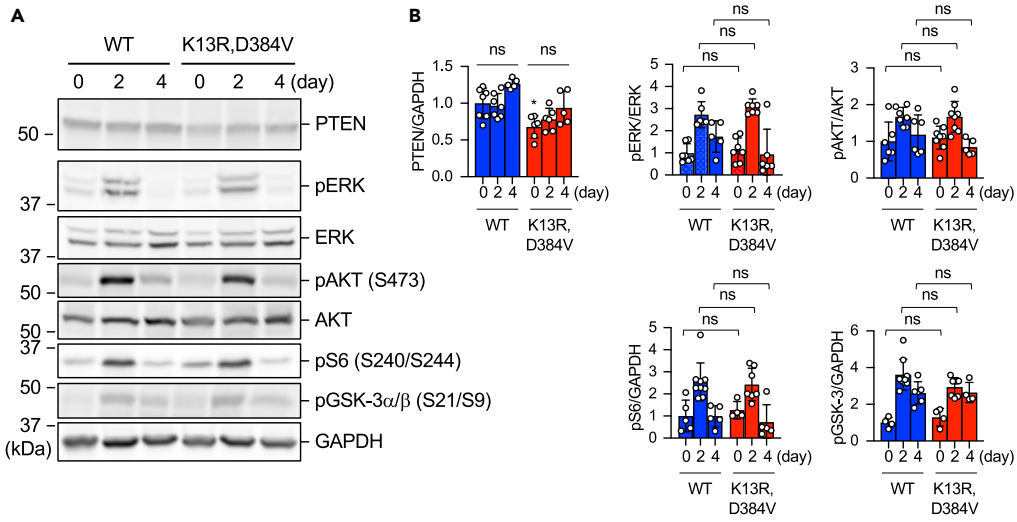

Figure 9. Phosphorylation of AKT, ERK, GSK-3, and Ribosomal Protein S6 Is Not Affected in the Liver of Nuclear PTEN-Deficient Mice

(A and B) Western blotting of livers dissected from WT and nuclear PTEN-deficient mice at the indicated days after CCl_4 injection using the indicated antibodies. Band intensity was quantified in (B). Bars are average ± SD (n = 4–9 livers). Statistical analysis was performed using one-way ANOVA with post hoc Tukey.

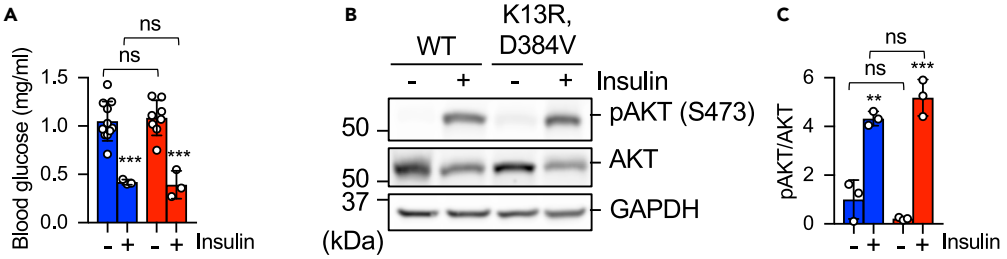

Figure 10. Nuclear PTEN-Deficient Mice Normally Respond to Insulin

(A) WT and nuclear PTEN-deficient mice were subjected to intraperitoneal injection of insulin (5 U/kg body weight). At 10 min after injection, blood glucose levels were measured. Bars are average ± SD (n = 3–11 mice).

(B and C) Western blotting of livers using antibodies to AKT, phospho-AKT (S473). Band intensity was quantified in (C). Bars are average ± SD (n = 3 livers). Statistical analysis was performed using one-way ANOVA with post hoc Tukey: **p < 0.01, ***p < 0.001.

DISCUSSION

Hepatocellular carcinoma is associated with persistent liver damages due to viral infections, environmental chemicals, excess alcohol consumption, and metabolic syndrome, such as non-alcoholic steatohepatitis, and is manifested by liver fibrosis or cirrhosis (Erstad et al., 2019; Mishra et al., 2009; Yang et al., 2019). *PTEN* has been shown to be mutated or lost in up to 30% of hepatocellular carcinoma (Khalid et al., 2017; Parikh et al., 2010). Also, decreased levels of PTEN are found in more than 50% of hepatocellular carcinoma and could be used as a prognostic marker (Khalid et al., 2017; Parikh et al., 2010). Therefore, it is important to understand the function of PTEN in the pathogenesis of hepatocellular carcinoma. Because PTEN has been shown to function in multiple locations (Baker, 2007; Gil et al., 2007; Hopkins and Parsons, 2014; Kreis et al., 2014; Leslie et al., 2016; Planchon et al., 2008), deciphering its functional importance at distinct subcellular locations will be critical to revealing how the loss of PTEN contributes to pathogenesis. In this study, we investigated the role of PTEN in the nucleus in hepatocellular carcinoma using a preclinical platform, in which hepatocellular carcinoma is induced by the combination of carcinogen (DEN) and repeated injection of the oxidative stress-inducing hepatotoxin (CCl_4). This mouse model induces extensive fibrosis in the liver, similar to human patients (Heindryckx et al., 2009; Uehara et al., 2014). We found that the formation of hepatocellular carcinoma was greatly accelerated in nuclear PTEN-deficient mice with increased DNA damage. These data provide the first *in vivo* evidence that nuclear PTEN mitigates the tumorigenesis by controlling DNA damage.

Although PTEN negatively controls PI3-kinase/AKT signaling as a lipid phosphatase at the plasma membrane and, therefore, total loss of PTEN enhances this oncogenic signaling pathway, nuclear PTEN-deficient mice maintain normal signaling involving AKT, mTOR, and ERK. Previous studies have reported that the loss of total PTEN in the liver in hepatocyte-specific PTEN knockout mice results in increase liver sizes and abnormality in insulin signaling due to increased PI3-kinase/AKT signaling (Horie et al., 2004; Stiles et al., 2004). These hepatocyte-specific *Pten* knockout mice also showed spontaneous adenomas and hepatocellular carcinoma at around 1 year old. Altered liver size and physiology and tumorigenesis in this mouse model likely involve a combination of consequences that are caused by the loss of PTEN functions in all of its subcellular locations. In contrast, nuclear PTEN-deficient mice showed a normal liver size and normal insulin response. Therefore, our data suggest that nuclear PTEN is unlikely to control the growth of the liver and glucose metabolism under normal conditions. Since nuclear PTEN-deficient mice do not produce spontaneous tumors until at least 1.5 years of age (Igarashi et al., 2018), nuclear PTEN plays an important role in protecting the liver from tumorigenesis when animals are exposed to stress and chronic liver damage.

CCl_4 is metabolized to highly reactive trichloromethyl radical by cytochrome p450, mainly in the liver, leading to oxidative stress and liver injuries (Recknagel et al., 1989; Sheweita et al., 2001). Our data suggest that K13 is important for the nuclear localization of PTEN as well as its nuclear accumulation in the liver under oxidative stress induced by CCl_4. Consistent with these *in vivo* data, K13 is important for the nuclear accumulation of PTEN in cell culture systems in response to H_2O_2. Using live-cell imaging with PTEN fused to photoconvertible mEos, we found that K13 controls the nuclear import of PTEN. Also, although WT PTEN decreases its nuclear export under oxidative stress, $PTEN_{K13R}$ was unable to decrease the nuclear export

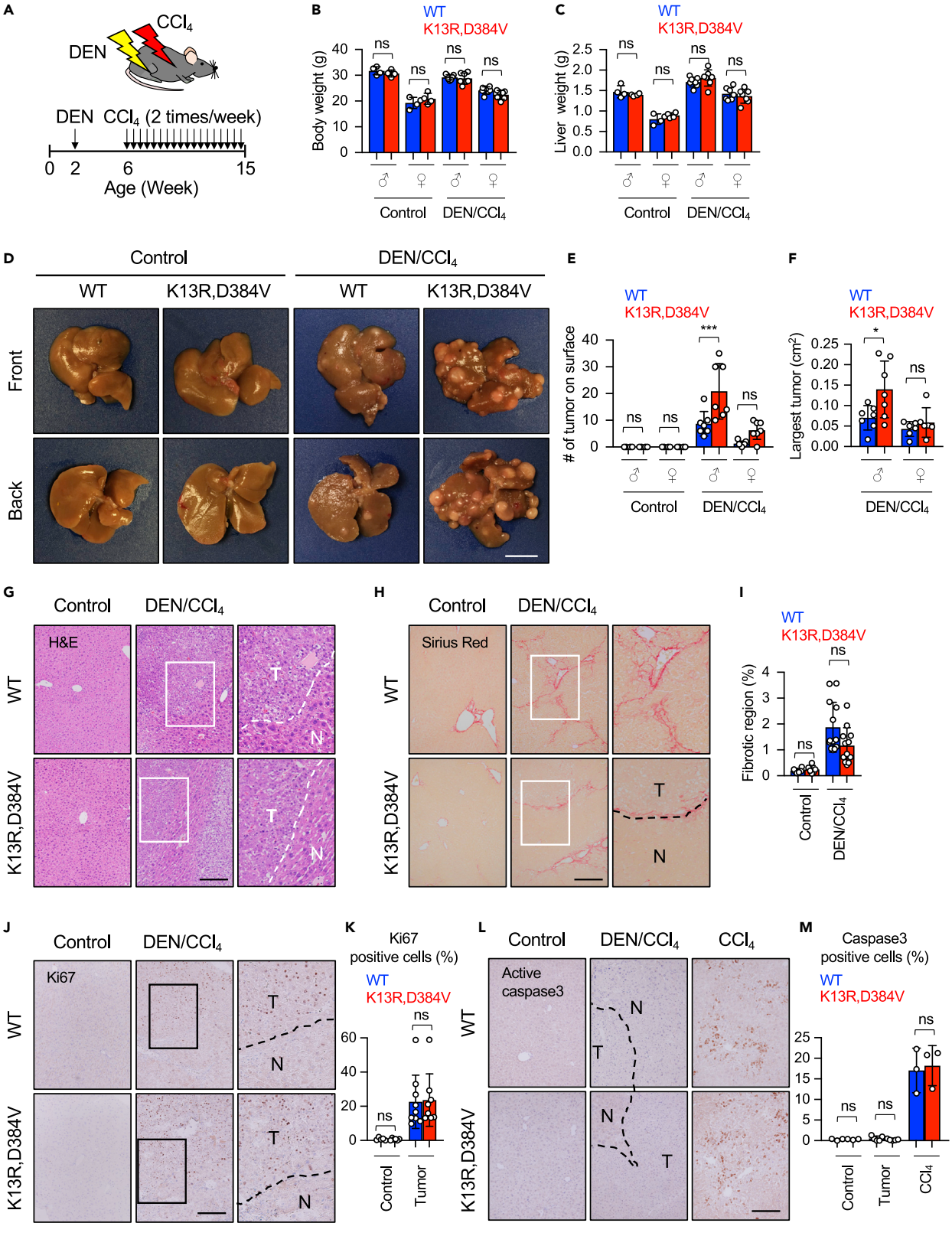
A
CCl4
DEN
DEN CCl4 (2 times/week)
0 2 6 15
Age (Week)
B
WT
K13R,D384V
Body weight (g)
ns
Control
DEN/CCl4
C
Liver weight (g)
D
Control
DEN/CCl4
WT
K13R,D384V
Front
Back
E
# of tumor on surface
***
F
Largest tumor (cm2)
*
G
H&E
T
N
H
Sirius Red
I
Fibrotic region (%)
J
Ki67
K
Ki67 positive cells (%)
L
Active caspase3
CCl4
M
Caspase3 positive cells (%)

Figure 11. Increased Hepatocarcinoma in Nuclear PTEN-Deficient Mice

(A) Experimental design for DEN/CCl_4-induced liver cancer in mice. WT and nuclear PTEN-deficient mice were subjected to intraperitoneal injection of DEN at 2 weeks of age. Mice were further treated with CCl_4 twice per week from 6 to 14 weeks of age. Mice were analyzed at 15 weeks.

(B and C) Weights of the body (B) and liver (C) (n = 4 male and 4 female mice for control, 7 male and 7 female mice for DEN/CCl_4-treated).

(D) Images of the front and back sides of livers that are isolated from male mice. Scale bar, 1 cm.

(E and F) The number of tumors (E) and the size of the largest tumors (F) observed on the surface of the livers were quantified. Bars are average ± SD (n = 4 male and 4 female mice for control, 7 male and 7 female mice for DEN/CCl_4-treated).

(G–M) Liver sections were subjected to H&E staining (G), Sirius red staining (H), Ki67 immunostaining (J), and active caspase-3 immunostaining (L). For active caspase-3, liver sections at 2 days after CCl_4 injection were also analyzed (CCl_4). T, tumors; N, non-tumor regions. Scale bars, 200 μm. (I) Fibrotic regions were quantified based on Sirius red staining. Bars are average ± SD (n = 6–13 livers). (K) Ki67-positive cells were quantified. Bars are average ± SD (n = 5–9 livers). (M) Active caspase-3-positive cells were quantified. Bars are average ± SD (n = 3–5 livers). Statistical analysis was performed using Student's t test in (B), (C), (E), (F), (I), (K) and (M): *$p < 0.05$, ***$p < 0.001$.

under oxidative stress. Therefore, K13 controls both the nuclear import rate at the basal condition and the modulation of the nuclear export rate in response to oxidative stress.

It has been shown that PTEN undergoes multiple post-translational modifications, such as SUMOylation, phosphorylation, ubiquitination, and acetylation (Kreis et al., 2014; Leslie et al., 2016). These modifications of PTEN regulate its subcellular localization, enzymatic activity, and protein stability. The multiple layers of regulation enable PTEN to function as an important tumor suppressor with multiple functions at different locations. In our experiments, K13 was critical for the dynamics of the nuclear localization and accumulation; however, we do not rule out the possibility that, under different physiological and pathological conditions, other lysines and residues could provide crucial regulatory mechanisms through different post-translational modifications. Supporting this notion, multiple ubiquitin E3 ligases, protein kinases, and other enzymes have been reported to modify PTEN in previous studies (Ge et al., 2020; Kreis et al., 2014; Leslie et al., 2016). These regulatory mechanisms could also cross talk and create a sophisticated regulatory network for PTEN. It would be of great interest to determine how different regulations affect each other in healthy cells and animals and how changes in the regulatory system drive the pathogenesis of cancers.

Limitation of the Study

First, we demonstrate that the nuclear localization of PTEN depends on its ubiquitination at lysine 13. However, we have not addressed what ubiquitin ligase mediates this post-translational modification. Second, we show that oxidative stress and DNA damage drive the accumulation of PTEN in the nucleus by decreasing its nuclear export. Yet it remains to be determined what machinery controls this export process. Third, although the lack of nuclear PTEN accelerates the formation of hepatocellular carcinoma that is induced by hepatotoxin and oxidative stress, it is unknown whether nuclear PTEN functions as a tumor suppressor in other types of cancers. We will address these questions in our future studies.

Resource Availability

Lead Contact

Miho Iijima (miijima@jhmi.edu).

Materials Availability

This study did not generate new reagents.

Data and Code Availability

All data are included in the published article and the Supplemental Information, and any additional information will be available from the lead contact upon request.

METHODS

All methods can be found in the accompanying Transparent Methods supplemental file.

SUPPLEMENTAL INFORMATION

Supplemental Information can be found online at https://doi.org/10.1016/j.isci.2020.101548.

ACKNOWLEDGMENTS

We thank past and present members of the Iijima and Sesaki labs for helpful discussions and technical assistance. We are grateful to Dr. Rong Li for providing the mEos3.2 plasmid. This work was supported by NIH grants to MI (GM131768 and NS114458) and HS (GM123266).

AUTHOR CONTRIBUTIONS

T.K., H.S., and M.I. conceived the project. T.K., T.Y., H.N., A.I., and M.I. performed the experiments. T.K., T.Y., H.N., A.I., R.A.A., H.S., and M.I. analyzed the data. T.K., T.Y., H.N., A.I., R.A.A., H.S., and M.I. contributed to discussions. T.K., H.S., and M.I. wrote the manuscript.

DECLARATIONS OF INTERESTS

The authors declare no competing interests.

Received: April 22, 2020
Revised: June 16, 2020
Accepted: September 7, 2020
Published: October 23, 2020

REFERENCES

Backman, S.A., Stambolic, V., Suzuki, A., Haight, J., Elia, A., Pretorius, J., Tsao, M.S., Shannon, P., Bolon, B., Ivy, G.O., et al. (2001). Deletion of Pten in mouse brain causes seizures, ataxia and defects in soma size resembling Lhermitte-Duclos disease. Nat. Genet. *29*, 396–403.

Baker, S.J. (2007). PTEN enters the nuclear age. Cell *128*, 25–28.

Bassi, C., Ho, J., Srikumar, T., Dowling, R.J., Gorrini, C., Miller, S.J., Mak, T.W., Neel, B.G., Raught, B., and Stambolic, V. (2013). Nuclear PTEN controls DNA repair and sensitivity to genotoxic stress. Science *341*, 395–399.

Chalhoub, N., and Baker, S.J. (2009). PTEN and the PI3-kinase pathway in cancer. Annu. Rev. Pathol. *4*, 127–150.

Chang, C.J., Mulholland, D.J., Valamehr, B., Mosessian, S., Sellers, W.R., and Wu, H. (2008). PTEN nuclear localization is regulated by oxidative stress and mediates p53-dependent tumor suppression. Mol. Cell. Biol. *28*, 3281–3289.

Choi, B.H., Chen, Y., and Dai, W. (2013). Chromatin PTEN is involved in DNA damage response partly through regulating Rad52 sumoylation. Cell Cycle *12*, 3442–3447.

Chung, J.H., Ostrowski, M.C., Romigh, T., Minaguchi, T., Waite, K.A., and Eng, C. (2006). The ERK1/2 pathway modulates nuclear PTEN-mediated cell cycle arrest by cyclin D1 transcriptional regulation. Hum. Mol. Genet. *15*, 2553–2559.

Das, S., Dixon, J.E., and Cho, W. (2003). Membrane-binding and activation mechanism of PTEN. Proc. Natl. Acad. Sci. U S A *100*, 7491–7496.

Endersby, R., and Baker, S.J. (2008). PTEN signaling in brain: neuropathology and tumorigenesis. Oncogene *27*, 5416–5430.

Erstad, D.J., Razavi, A.A., Li, S., Tanabe, K.K., and Fuchs, B.C. (2019). Prevention strategies for hepatocellular carcinoma. In Hepatocellular Carcinoma: Translational Precision Medicine Approaches, Y. Hoshida, ed. (Springer), pp. 255–289.

Fruman, D.A., Chiu, H., Hopkins, B.D., Bagrodia, S., Cantley, L.C., and Abraham, R.T. (2017). The PI3K pathway in human disease. Cell *170*, 605–635.

Ge, M.K., Zhang, N., Xia, L., Zhang, C., Dong, S.S., Li, Z.M., Ji, Y., Zheng, M.H., Sun, J., Chen, G.Q., et al. (2020). FBXO22 degrades nuclear PTEN to promote tumorigenesis. Nat. Commun. *11*, 1720.

Gil, A., Andres-Pons, A., and Pulido, R. (2007). Nuclear PTEN: a tale of many tails. Cell Death Differ. *14*, 395–399.

Heindryckx, F., Colle, I., and Van Vlierberghe, H. (2009). Experimental mouse models for hepatocellular carcinoma research. Int. J. Exp. Pathol. *90*, 367–386.

Hopkins, B.D., and Parsons, R.E. (2014). Molecular pathways: intercellular PTEN and the potential of PTEN restoration therapy. Clin. Cancer Res. *20*, 5379–5383.

Horie, Y., Suzuki, A., Kataoka, E., Sasaki, T., Hamada, K., Sasaki, J., Mizuno, K., Hasegawa, G., Kishimoto, H., Iizuka, M., et al. (2004). Hepatocyte-specific Pten deficiency results in steatohepatitis and hepatocellular carcinomas. J. Clin. Invest. *113*, 1774–1783.

Hou, B., Xu, S., Xu, Y., Gao, Q., Zhang, C., Liu, L., Yang, H., Jiang, X., and Che, Y. (2019). Grb2 binds to PTEN and regulates its nuclear translocation to maintain the genomic stability in DNA damage response. Cell Death Dis. *10*, 546.

Igarashi, A., Itoh, K., Yamada, T., Adachi, Y., Kato, T., Murata, D., Sesaki, H., and Iijima, M. (2018). Nuclear PTEN deficiency causes microcephaly with decreased neuronal soma size and increased seizure susceptibility. J. Biol. Chem. *293*, 9292–9300.

Iijima, M., and Devreotes, P. (2002). Tumor suppressor PTEN mediates sensing of chemoattractant gradients. Cell *109*, 599–610.

Iijima, M., Huang, Y.E., and Devreotes, P. (2002). Temporal and spatial regulation of chemotaxis. Dev. Cell *3*, 469–478.

Khalid, A., Hussain, T., Manzoor, S., Saalim, M., and Khaliq, S. (2017). PTEN: a potential prognostic marker in virus-induced hepatocellular carcinoma. Tumour Biol. *39*, 1010428317705754.

Knobbe, C.B., Lapin, V., Suzuki, A., and Mak, T.W. (2008). The roles of PTEN in development, physiology and tumorigenesis in mouse models: a tissue-by-tissue survey. Oncogene *27*, 5398–5415.

Kreis, P., Leondaritis, G., Lieberam, I., and Eickholt, B.J. (2014). Subcellular targeting and dynamic regulation of PTEN: implications for neuronal cells and neurological disorders. Front. Mol. Neurosci. *7*, 23.

Kwon, C.H., Luikart, B.W., Powell, C.M., Zhou, J., Matheny, S.A., Zhang, W., Li, Y., Baker, S.J., and Parada, L.F. (2006). Pten regulates neuronal arborization and social interaction in mice. Neuron *50*, 377–388.

Leslie, N.R., Kriplani, N., Hermida, M.A., Alvarez-Garcia, V., and Wise, H.M. (2016). The PTEN protein: cellular localization and post-translational regulation. Biochem. Soc. Trans. *44*, 273–278.

Ma, J., Benitez, J.A., Li, J., Miki, S., Ponte de Albuquerque, C., Galatro, T., Orellana, L., Zanca, C., Reed, R., Boyer, A., et al. (2019). Inhibition of nuclear PTEN tyrosine phosphorylation enhances glioma radiation sensitivity through attenuated DNA repair. Cancer Cell *36*, 690–691.

Mishra, L., Banker, T., Murray, J., Byers, S., Thenappan, A., He, A.R., Shetty, K., Johnson, L., and Reddy, E.P. (2009). Liver stem cells and hepatocellular carcinoma. Hepatology *49*, 318–329.

Naugler, W.E., Sakurai, T., Kim, S., Maeda, S., Kim, K., Elsharkawy, A.M., and Karin, M. (2007). Gender disparity in liver cancer due to sex differences in MyD88-dependent IL-6 production. Science *317*, 121–124.

Nguyen, H.N., Afkari, Y., Senoo, H., Sesaki, H., Devreotes, P.N., and Iijima, M. (2014a). Mechanism of human PTEN localization revealed by heterologous expression in Dictyostelium. Oncogene *33*, 5688–5696.

Nguyen, H.N., Yang, J.M., Afkari, Y., Park, B.H., Sesaki, H., Devreotes, P.N., and Iijima, M. (2014b). Engineering ePTEN, an enhanced PTEN with increased tumor suppressor activities. Proc. Natl. Acad. Sci. U S A *111*, E2684–E2693.

Nguyen, H.N., Yang, J.M., Jr., Rahdar, M., Keniry, M., Swaney, K.F., Parsons, R., Park, B.H., Sesaki, H., Devreotes, P.N., and Iijima, M. (2015a). A new class of cancer-associated PTEN mutations defined by membrane translocation defects. Oncogene *34*, 3737–3743.

Nguyen, H.N., Yang, J.M., Miyamoto, T., Itoh, K., Rho, E., Zhang, Q., Inoue, T., Devreotes, P.N., Sesaki, H., and Iijima, M. (2015b). Opening the conformation is a master switch for the dual localization and phosphatase activity of PTEN. Sci. Rep. *5*, 12600.

Papa, A., Wan, L., Bonora, M., Salmena, L., Song, M.S., Hobbs, R.M., Lunardi, A., Webster, K., Ng, C., Newton, R.H., et al. (2014). Cancer-associated PTEN mutants act in a dominant-negative manner to suppress PTEN protein function. Cell *157*, 595–610.

Parikh, A., Miranda, E.R., Katoh-Kurasawa, M., Fuller, D., Rot, G., Zagar, L., Curk, T., Sucgang, R., Chen, R., Zupan, B., et al. (2010). Conserved developmental transcriptomes in evolutionarily divergent species. Genome Biol. *11*, R35.

Planchon, S.M., Waite, K.A., and Eng, C. (2008). The nuclear affairs of PTEN. J. Cell Sci. *121*, 249–253.

Rahdar, M., Inoue, T., Meyer, T., Zhang, J., Vazquez, F., and Devreotes, P.N. (2009). A phosphorylation-dependent intramolecular interaction regulates the membrane association and activity of the tumor suppressor PTEN. Proc. Natl. Acad. Sci. U S A *106*, 480–485.

Recknagel, R.O., Glende, E.A., Jr., Dolak, J.A., and Waller, R.L. (1989). Mechanisms of carbon tetrachloride toxicity. Pharmacol. Ther. *43*, 139–154.

Shen, W.H., Balajee, A.S., Wang, J., Wu, H., Eng, C., Pandolfi, P.P., and Yin, Y. (2007). Essential role for nuclear PTEN in maintaining chromosomal integrity. Cell *128*, 157–170.

Sheweita, S.A., El-Gabar, M.A., and Bastawy, M. (2001). Carbon tetrachloride changes the activity of cytochrome P450 system in the liver of male rats: role of antioxidants. Toxicology *169*, 83–92.

Song, M.S., Carracedo, A., Salmena, L., Song, S.J., Egia, A., Malumbres, M., and Pandolfi, P.P. (2011). Nuclear PTEN regulates the APC-CDH1 tumor-suppressive complex in a phosphatase-independent manner. Cell *144*, 187–199.

Song, M.S., Salmena, L., Carracedo, A., Egia, A., Lo-Coco, F., Teruya-Feldstein, J., and Pandolfi, P.P. (2008). The deubiquitinylation and localization of PTEN are regulated by a HAUSP-PML network. Nature *455*, 813–817.

Song, M.S., Salmena, L., and Pandolfi, P.P. (2012). The functions and regulation of the PTEN tumour suppressor. Nat. Rev. Mol. Cell Biol. *13*, 283–296.

Stiles, B., Wang, Y., Stahl, A., Bassilian, S., Lee, W.P., Kim, Y.J., Sherwin, R., Devaskar, S., Lesche, R., Magnuson, M.A., et al. (2004). Liver-specific deletion of negative regulator Pten results in fatty liver and insulin hypersensitivity [corrected]. Proc. Natl. Acad. Sci. U S A *101*, 2082–2087.

Trotman, L.C., Wang, X., Alimonti, A., Chen, Z., Teruya-Feldstein, J., Yang, H., Pavletich, N.P., Carver, B.S., Cordon-Cardo, C., Erdjument-Bromage, H., et al. (2007). Ubiquitination regulates PTEN nuclear import and tumor suppression. Cell *128*, 141–156.

Uehara, T., Pogribny, I.P., and Rusyn, I. (2014). The DEN and CCl4 -induced mouse model of fibrosis and inflammation-associated hepatocellular carcinoma. Curr. Protoc. Pharmacol. *66*, 14 30 11–10.

Yang, J.-M., Schiapparelli, P., Nguyen, H., Igarashi, A., Zhang, Q., Abbadi, S., Amzel, L., Sesaki, H., Quiñones-Hinojosa, A., and Iijima, M. (2017). Characterization of PTEN mutations in brain cancer reveals that pten mono-ubiquitination promotes protein stability and nuclear localization. Oncogene *36*, 3673–3685.

Yang, J.D., Hainaut, P., Gores, G.J., Amadou, A., Plymoth, A., and Roberts, L.R. (2019). A global view of hepatocellular carcinoma: trends, risk, prevention and management. Nat. Rev. Gastroenterol. Hepatol. *16*, 589–604.

Zhang, M., Chang, H., Zhang, Y., Yu, J., Wu, L., Ji, W., Chen, J., Liu, B., Lu, J., Liu, Y., et al. (2012). Rational design of true monomeric and bright photoactivatable fluorescent proteins. Nat. Methods *9*, 727–729.

iScience, Volume *23*

Supplemental Information

The Loss of Nuclear PTEN Increases Tumorigenesis in a Preclinical Mouse Model for Hepatocellular Carcinoma

Takashi Kato, Tatsuya Yamada, Hideki Nakamura, Atsushi Igarashi, Robert A. Anders, Hiromi Sesaki, and Miho Iijima

Supplemental Information

The Loss of Nuclear PTEN Increases Tumorigenesis in a Preclinical Mouse Model for Hepatocellular Carcinoma

Takashi Kato, Tatsuya Yamada, Hideki Nakamura, Atsushi Igarashi, Robert A. Anders, Hiromi Sesaki and Miho Iijima

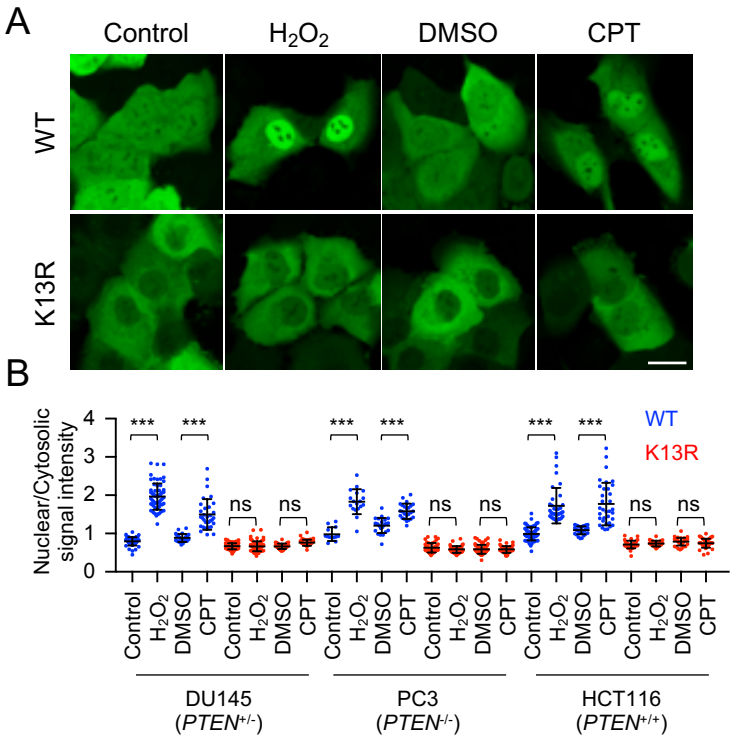

Supplementary Figure 1. No effects of endogenous PTEN on the nuclear localization of ectopic PTEN-GFP. (A and B) DU145 cells, PC3 cells, and HCT116 cells, all of which express either PTEN-GFP or $PTEN_{K13R}$-GFP, were treated with 0.5 mM H_2O_2 for 1 h or 50 µM camptothecin for 6 h. Images of DU145 cells are presented in (A). The intensity of phospho-PTEN was quantified relative to that of PTEN in (B). Bars are average ± SD (n = 13–72 cells). Statistical analysis was performed using one-way ANOVA with post-hoc Tukey: ***p < 0.001.

Plasmids	References
pcDNA3.1-PTEN-GFP	Nguyen et al (2015), Yang et al (2017)
pcDNA3.1-PTEN(K6R)-GFP	This study
pcDNA3.1-PTEN(K13R)-GFP	Nguyen et al (2015), Yang et al (2017)
pcDNA3.1-PTEN(K66R)-GFP	This study
pcDNA3.1-PTEN(K80R)-GFP	This study
pcDNA3.1-PTEN(K254R)-GFP	This study
pcDNA3.1-PTEN(K260R,K263R,K266R,K267R,K269R)-GFP	This study
pcDNA3.1-PTEN(K289R)-GFP	This study
pcDNA3.1-PTEN(T319A,T321A)-GFP	Yang et al (2017)
pcDNA3.1-PTEN(T366A,S370A)-GFP	Yang et al (2017)
pcDNA3.1-PTEN(S380A,T382A,T383A,S385A)-GFP	Nguyen et al (2015), Yang et al (2017)
pcDNA3.1-PTEN(K0)-GFP	This study
pcDNA3.1-PTEN(K0K13)-GFP	This study
pcDNA3.1-PTEN(K13-Ubiquitin)-GFP	This study
pRK5-HA-Ubiquitin-WT	Addgene #17608
pEGFP-C1	Clontech
pCAGGS1-PTEN-mEOS3.2	This study
pCAGGS1-PTEN(K13R)-mEOS3.2	This study
pInducer20-PTEN-GFP	This study
pInducer20-PTEN(K13R)-GFP	This study

Supplementary Table 1

Transparent Methods

Animals

All animal work was performed according to the guideline established by the Johns Hopkins University Committee on Animal Care. Heterozygous PTEN knockout mice were generated by crossing *Pten*^{flox} mice (Stock No: 006440, Jackson Laboratory) and *CMV-Cr*e mice (Stock No: 006054). The *CMV-Cre* transgene was removed by further crosses. Nuclear PTEN-deficient mice that carry the K13R and D384V mutations have been previously described (Igarashi et al., 2018). To obtain littermate control and mutant mice, heterozygous nuclear PTEN-deficient mice were bred. To induce liver damage, we intraperitoneally injected 20% CCl_4/mineral oil (10 ml/kg body weight; 289116, Sigma-Aldrich) into WT and nuclear PTEN-deficient mice at 2–3 months of age. To induce liver cancer, we intraperitoneally injected DEN (25 mg/kg body weight; N0258, Sigma-Aldrich) into WT and nuclear PTEN-deficient mice at 2 weeks of age, and then intraperitoneally injected 20% CCl_4/mineral oil (2.5 ml/kg body weight) twice a week from 6 to 14 week of age (Heindryckx et al., 2009; Uehara et al., 2014).

Cells

HEK293T and HepG2 cells were cultured in the DMEM medium (D5796, Sigma-Aldrich) containing 10% FBS (F4135, Sigma-Aldrich) and 1% penicillin/streptomycin (15140-122, Gibco). HepG2, DU145, HCT116, and PC3 cells were obtained from the American Type Culture Collection. DU145, HCT116, and PC3 cells were maintained in the RPMI medium 1640 (11875-093, Gibco) containing 10% FBS and 1% penicillin/streptomycin.

Plasmids and lentiviruses

The plasmids are listed in Supplemental Table S1. To express PTEN-GFP constructs in HEK293T and HCT116 cells, plasmid transfection was performed with Lipofectamine3000 (L3000015, Invitrogen). To express PTEN-GFP constructs in HepG2, DU145 cells, and PC3 cells, lentiviruses expressing PTEN-GFP constructs from the doxycycline-inducible promoter were used. The expression of PTEN was induced by 0.1 μg/ml doxycycline (D9851, Sigma-Aldrich) overnight. To express PTEN-mEos in DU145 cells, plasmid transfection was used.

Lentiviruses were produced as described previously (Yamada et al., 2018). The pInducer20 plasmids carrying PTEN constructs were cotransfected into HEK293T cells with two other plasmids, pCMV-ΔR8.9 and pCMV-VSVG, using Lipofectamine3000. Two days after transfection, the supernatant of the transfected cells containing released viruses was collected. The viruses were quick-frozen in liquid nitrogen and stored at -80°C.

Reagents

H_2O_2 (216763), camptothecin (C9911), SPNO (S150), and GSH-MEE (G1404) were purchased from Sigma. PR-610 was obtained from Millipore (662141).

Antibodies

The primary antibodies used in this study were: PTEN (9559, Cell Signaling Technology [CST]), phospho-PTEN (S380/T382/T383) (9549, CST), phospho-PTEN (S380) (9551, CST), phospho-PTEN (S385) (07-890-I, EMD Millipore), AKT (9272, CST), phospho-AKT (4060, CST), ERK (9107, CST), phospho-ERK (4370, CST), phospho-S6 (S240/244) (5364, CST), phospho-GSK-3α/ß (S21/9)

(9331, CST), GAPDH (MA5-15738, Invitrogen), Ki67 (M7249, DAKO), phospho-H2AX (S139) (ab11174, Abcam), and active caspase-3 (AF835, R&D System). The fluorescently-labeled secondary antibodies were obtained from Invitrogen: Alexa488 anti-rabbit IgG (A21206), Alexa488 anti-mouse IgG (A21202), Alexa568 anti-rat IgG (A11077), Alexa647 anti-rabbit IgG (A31573), and Alexa647 anti-mouse IgG (A31571). HRP-conjugated anti-rat IgG (474-1612, KPL) was obtained from Sera Care. HRP-conjugated anti-rabbit IgG (NA934V) was purchased from GE Healthcare.

Immunofluorescence for cultured cells

Cells were fixed in methanol for 20 min at -20°C. After washes with PBS, the cells were incubated in PBS containing 0.05% Tween 20 (PBS-T) supplemented with 3% BSA for 1 h. The cells were then incubated with anti-PTEN antibodies overnight at 4°C. After washes with PBS-T, samples were incubated with appropriate fluorescently-labeled secondary antibodies at room temperature for 1 h. Nuclear DNA was stained with 1 μg/ml DAPI (10236276001, Roche). Samples were observed on a LSM800 GaAsP laser scanning confocal microscope with the Zen software (Zeiss).

Photoconversion of PTEN-mEos

Cells expressing PTEN-mEos or $PTEN_{K13R}$-mEos were seeded in 8-well chambered coverglasses and cultured for 24 h. mEos in a region of the nucleus (5 μm^2) or two regions of the cytosol (2 × 5 μm^2) was photoconverted by a 405 nm laser on LSM800 GaAsP laser scanning confocal microscope (Zeiss). Images were obtained for both unconverted and photoconverted mEos

signals before photoconversion and every 5 min for 30 min after photoconversion. To analyze the effect of oxidative stress, 0.5 mM H_2O_2 was added to the culture medium 5 min prior to photoconversion.

Isolation of hepatocytes

Mice were anesthetized by intraperitoneal injection of Avertin (200 mg/kg). After the skin and abdominal muscle were incised, a cannula (25G) was inserted into the portal vein. The chest was incised, and the thoracic inferior vena cava was cut. Pre-warmed (37°C) HBSS (50 ml) (14185-052, Gibco) supplemented with 0.5 mM EDTA was first perfused to confirm no leakage. Then, 30 ml of the collagenase solution (DMEM medium containing 0.8 mg/ml collagenase I, 17018-029, Thermo Fisher) was perfused. Livers were dissected out and further incubated in 20 ml of the collagenase solution at 37°C for 15 min. Livers were transferred to a plastic culture dish, finely chopped with a surgical scissor, and pipetted up and down twice in 10 ml of HBSS supplemented with 0.5 mM EDTA. The chopped livers were filtered (70-µm pore size: 22363548, Thermo Fisher) and centrifuged at 50 × g for 3 min at 4°C to collect hepatocytes. The hepatocytes were washed twice in the DMEM medium by centrifugation. The hepatocytes were resuspended in the Williams' medium E (A1217601, Gibco) supplemented with Hepatocyte Thawing and Plating Supplement Pack (CM3000, Gibco). Hepatocytes (10,000) were plated on an 8-well chambered coverglass, which had been coated with 0.3% collagen (I) (A1048301, Gibco) in 0.02 N acetic acid for 10 min and washed with PBS (D8537, Sigma-Aldrich) three times.

Immunoprecipitation for PTEN-GFP

HEK293T cells were plated in 6-cm dishes and transfected with two plasmids carrying PTEN-GFP and HA-ubiquitin the next day. After 24 h, cells were harvested and homogenized by RIPA buffer (9806, CST), including a complete protease inhibitor cocktail (1697498001, Roche) and N-ethylmaleimide (E5876, Sigma-Aldrich). After centrifugation at 16,000 × g at 4°C for 10 min, the supernatants were incubated with GFP-Trap agarose beads (gta-20, Chromotek) for 3–4 h at 4°C with gentle rotation. After washes, the bound proteins were eluted with SDS-PAGE sample buffer.

Western blotting

Mouse liver tissues were homogenized in the RIPA buffer (9806, CST) containing complete protease inhibitor cocktail (1697498001, Roche) and phosphatase inhibitor cocktails (P5726 and P0044, Sigma-Aldrich). Lysates were centrifuged at 16,000 × g for 10 min, and the supernatants were collected. Proteins were separated using SDS-PAGE and then transferred onto Immobilon-FL (IPFL00010, EMD Millipore). After blocking in 3% BSA/PBS-T for 1 h at room temperature, the membranes were incubated with the primary antibodies overnight at 4°C. After washing with PBS-T, immunocomplexes were visualized using appropriate fluorescent-labeled secondary antibodies and detected using a PharosFX Plus molecular imager (Bio-Rad).

ALT Activity

The ALT activity in the blood was measured using the ALT Activity Assay Kit (MAK052, Sigma-Aldrich) according to the manufacturer's instruction.

Immunofluorescence microscopy and histology of livers

For immunofluorescence microscopy, mice were anesthetized by intraperitoneal injection of Avertin and fixed by cardiac perfusion of ice-cold 4% paraformaldehyde in PBS, as previously described (Igarashi et al., 2018; Yamada et al., 2018). The livers were dissected and further fixed in 4% paraformaldehyde in PBS for 3 h at 4°C. The samples were incubated in PBS containing 30% sucrose overnight and frozen in O.C.T. compound (23-730-571, Fisher Scientific) in a Tissue-Tek Cryomold (4566, Sakura Finetek USA). Frozen tissue blocks were sectioned and mounted on Superfrost Plus Microscope Slides (12-550-15, Fisher Scientific). Sections were subjected to antigen retrieval with 1 mM EDTA using a microwave oven and incubated with the primary antibodies at 4°C overnight. After washes with PBS-T, the samples were incubated with appropriate fluorescently-labeled secondary antibodies at room temperature for 1 h. DAPI (1 μg/ml) was used to stain nuclear DNA.

For histology, fixed livers were embedded in paraffin at Johns Hopkins School of Medicine Pathology Core. Paraffin sections were cut, and H&E stained at the Pathology Core. The samples were viewed using a microscope (model BX51, Olympus) equipped with a DP-70 color camera. To analyze fibrosis, paraffin sections were stained with Picro Sirius Red Stain Kit (ab150681, Abcam) according to the manufacturer's instruction. To immunostain Ki67 and active caspase-3, paraffin sections were deparaffinized, subjected to antigen retrieval with 1 mM EDTA using a pressure cooker for 15 min, and incubated with the primary antibody at 4°C overnight. After washes with PBS-T, the samples were incubated with HRP-conjugated

secondary antibody for 1 h at room temperature and stained with DAB (ab64238, Abcam).

Hematoxylin (MHS16, Sigma-Aldrich) was used to counterstain nuclei.

Supplementary References

Heindryckx, F., Colle, I., and Van Vlierberghe, H. (2009). Experimental mouse models for hepatocellular carcinoma research. Int J Exp Pathol *90*, 367-386.
Igarashi, A., Itoh, K., Yamada, T., Adachi, Y., Kato, T., Murata, D., Sesaki, H., and Iijima, M. (2018). Nuclear PTEN deficiency causes microcephaly with decreased neuronal soma size and increased seizure susceptibility. J Biol Chem *293*, 9292-9300.
Uehara, T., Pogribny, I.P., and Rusyn, I. (2014). The DEN and CCl4 -Induced Mouse Model of Fibrosis and Inflammation-Associated Hepatocellular Carcinoma. Curr Protoc Pharmacol *66*, 14 30 11-10.
Yamada, T., Murata, D., Adachi, Y., Itoh, K., Kameoka, S., Igarashi, A., Kato, T., Araki, Y., Huganir, R.L., Dawson, T.M.*, et al.* (2018). Mitochondrial Stasis Reveals p62-Mediated Ubiquitination in Parkin-Independent Mitophagy and Mitigates Nonalcoholic Fatty Liver Disease. Cell Metab *28*, 588-604.